Title

Regulation of flagellar motility by the conserved flagellar protein CG34110/Ccdc135/FAP50

Journal

Molecular Biology of the Cell, 22(7)

ISSN

1059-1524

Authors

Yang, Yong
Cochran, Deborah A
Gargano, Mary D
et al.

Publication Date

2011-04-01

DOI

10.1091/mbc.e10-04-0331

Peer reviewed

Regulation of flagellar motility by the conserved flagellar protein CG34110/Ccdc135/FAP50

Yong Yang[a], Deborah A. Cochran[b], Mary D. Gargano[a], Iryna King[a], Nayef K. Samhat[a], Benjain P. Burger[a], Katherine R. Sabourin[a], Yuqing Hou[b], Junya Awata[b], David A.D. Parry[c], Wallace F. Marshall[d], George B. Witman[b], and Xiangyi Lu[a]

[a]Institute of Environmental Health Sciences and Department of Biochemistry and Molecular Biology, Wayne State University, Detroit, MI 48201; [b]Department of Cell Biology, University of Massachusetts Medical School, Worcester, MA 01655; [c]Institute of Fundamental Sciences and the Riddet Institute, Massey University, Palmerston North 4442, New Zealand; [d]Department of Biochemistry and Biophysics, University of California at San Francisco, San Francisco, CA 94143

ABSTRACT **Eukaryotic cilia and flagella are vital sensory and motile organelles. The calcium channel PKD2 mediates sensory perception on cilia and flagella, and defects in this can contribute to ciliopathic diseases. Signaling from Pkd2-dependent Ca^{2+} rise in the cilium to downstream effectors may require intermediary proteins that are largely unknown. To identify these proteins, we carried out genetic screens for mutations affecting *Drosophila melanogaster* sperm storage, a process mediated by *Drosophila Pkd2*. Here we show that a new mutation *lost boys* (*lobo*) encodes a conserved flagellar protein CG34110, which corresponds to vertebrate Ccdc135 (E = 6e-78) highly expressed in ciliated respiratory epithelia and sperm, and to FAP50 (E = 1e-28) in the *Chlamydomonas reinhardtii* flagellar proteome. CG34110 localizes along the fly sperm flagellum. FAP50 is tightly associated with the outer doublet microtubules of the axoneme and appears not to be a component of the central pair, radial spokes, dynein arms, or structures defined by the *mbo* waveform mutants. Phenotypic analyses indicate that both *Pkd2* and *lobo* specifically affect sperm movement into the female storage receptacle. We hypothesize that the CG34110/Ccdc135/FAP50 family of conserved flagellar proteins functions within the axoneme to mediate Pkd2-dependent processes in the sperm flagellum and other motile cilia.**

Monitoring Editor
Julie A. Brill
The Hospital for Sick Children

Received: Apr 21, 2010
Revised: Jan 18, 2011
Accepted: Jan 25, 2011

INTRODUCTION

Cilia and flagella are evolutionarily homologous cell organelles, with cilium being a generic term for either a motile or nonmotile axoneme-containing protrusion and a flagellum being a motile cilium used for locomotion (Mitchell, 2007; Satir *et al.*, 2008). Recent studies have shown that most cells have one or more cilia that mediate sensory perception and fluid homeostasis necessary for normal development and physiology of living systems (Baker and Beales, 2009; Mirzadeh *et al.*, 2010; Vogel *et al.*, 2010; Wilson *et al.*, 2010). Ciliary dysfunction results in a variety of ciliopathic diseases, including many that are caused by abnormal motility of motile cilia (Baker and Beales, 2009). During evolution, cilium motility-dependent functions have expanded beyond swimming, food gathering, and parasitism in unicellular organisms to many more complex fluid-driven cellular processes in vertebrates, including humans. For example, the nodal cilia generate a directional flow that provides positional cues to the surrounding cells, leading to left–right body asymmetry in the developing embryos. Disruption of the nodal flow leads to *situs inversus* with mispositioning and malformation of internal organs (Okada *et al.*, 1999). The motile cilia of ependymal cells generate a flow of cerebrospinal fluid that plays roles in neuronal migration to the olfactory lobes (Sawamoto *et al.*, 2006). Disruption of the cerebrospinal fluid flow affects the neuronal migration and also causes fluid retention and hydrocephalus (Sawamoto *et al.*, 2006; Lechtreck *et al.*, 2008; Wilson *et al.*, 2010). In the reproductive tract, abnormal motility of motile cilia may cause ectopic pregnancy (Lyons *et al.*, 2006). Abnormal motility of the airway cilia leads to

This article was published online ahead of print in MBoC in Press (http://www.molbiolcell.org/cgi/doi/10.1091/mbc.E10-04-0331) on February 2, 2011.

Address correspondence to: Xiangyi Lu (xlu@wayne.edu).

Abbreviations used: CP, central pair microtubules; DSR, distal storage receptacle; ED, ejaculatory duct; ODs, outer doublet microtubules; PSR, proximal storage receptacle; 3R, right arm of the third chromosome; SR, seminal or storage receptacle; SV, seminal vesicle.

inefficient mucociliary clearance and respiratory problems (Braiman and Priel, 2008). To accomplish these diverse physiological roles, motile cilia and flagella exhibit a large repertoire of waveforms and are capable of versatile motility changes in response to the external environment (Gibbons, 1981).

A well-known mechanism for eliciting motility changes is alteration of intraflagellar Ca^{2+} concentrations (Kaupp *et al.*, 2008; King, 2010). This has been shown for ciliary reversal in *Paramecium* (Naito and Kaneko, 1972), reversal of flagellar bending chirality in various sperm (Ishijima and Hamaguchi, 1993; Kaupp *et al.*, 2008), sperm hyperactivation and chemotaxis (Publicover *et al.*, 2008), and waveform conversion from the asymmetric ciliary form to the symmetric flagellar form in the green alga *Chlamydomonas reinhardtii* (Schmidt and Eckert, 1976; Bessen *et al.*, 1980). Aside from inducing alternative waveforms, intraflagellar calcium can also reverse the flagellar wave propagation direction along the longitudinal axis of the axoneme (Sugrue *et al.*, 1988; Ishijima *et al.*, 1994). Whereas flagellar waves of most protozoa and spermatozoa start at the base and propagate toward the tip, some species, such as the Tephritid fly and the marine invertebrates *Myzostomum* and *Turritella*, have flagella that can propagate waves in both axial directions (Baccetti *et al.*, 1989; Ishijima *et al.*, 1994, 1999). Trypanosomes are unicellular parasites that use their singular flagella for movement in host tissues. Trypanosome flagella are unique in that they routinely propagate tip-to-base waves, which generate a flagellum-tip-leading, forward movement (Walker, 1961; Sugrue *et al.*, 1988; Hill, 2003). However, in response to lights or obstacles, trypanosome flagella initiate short bursts of base-to-tip waves that generate a backward movement. Flagellar waveform conversion or reversal of wave direction provides a means of backing up, reorienting the cell, and avoiding obstacles in physiological settings.

The axoneme of nearly all motile cilia and flagella has the canonical "9+2" structure (Porter and Sale, 2000; Heuser *et al.*, 2009). The cylindrical wall of the axoneme consists of nine outer doublet microtubules (ODs) that enclose a central pair (CP) of singlet microtubules in the center, extending from the basal body to the distal tip. Serving as interconnecting structures between the ODs and the CP are radial spokes, which are anchored along the lengths of each of the nine ODs and project toward the CP. The radial spokes are known to interact with regulatory proteins located on the CP and to relay signals back to the dynein motors that are anchored on the ODs (Smith, 2002b; Smith and Yang, 2004; Mitchell, 2004). The isolated demembranated axonemes of *C. reinhardtii* and *Crithidia oncopelti* have been shown to execute reversible waveform conversion and wave direction reversal, respectively, when reactivated in solutions of varying free Ca^{2+} concentrations (Bessen *et al.*, 1980; Sugrue *et al.*, 1988). This indicates that the mediators for waveform conversion and wave direction reversal are located on the axoneme. Many calcium-sensing proteins are integrated within the CP, radial spokes, and dynein motors (Smith, 2002a; Smith and Yang, 2004; Dymek and Smith, 2007). Although less is known about calcium-sensing or responding proteins on the ODs, three *C. reinhardtii mbo* (*move backward only*) mutations result in the loss of six to eight OD-associated polypeptides, and these mutant flagella are unable to execute waveform conversion (Segal *et al.*, 1984). The cloned *mbo2* locus encodes a conserved coiled-coil protein on the ODs with yet undefined functions in other organisms (Tam and Lefebvre, 2002).

The PKD2 family of calcium channels has been shown to function in motile as well as immotile cilia. Mutations in vertebrate *PKD2* lead to renal cystic growth (Wu *et al.*, 1998) and defects in left–right body asymmetry (Pennekamp *et al.*, 2002) due to disruptions of fluid sensation by the kidney and nodal cilia, respectively. The mating defect of *Caenorhabditis elegans Pkd2* is due to the loss of mechanosensation by the ciliated sensory neurons that mediate vulva location during mating (Barr and Sternberg, 1999). A working model applicable to these situations is that mechanical depression/bending of cilia opens the PKD2 channels on the ciliary membranes, which results in calcium influx into the cilia; this eventually leads to signal transduction and physiological changes in the cell body. It is unclear whether this ciliary bending model applies to *C. reinhardtii* and *Drosophila* where Pkd2 functions on flagella that are constantly beating (Gao *et al.*, 2003; Watnick *et al.*, 2003; Huang *et al.*, 2007).

The *C. reinhardtii* PKD2 (CrPKD2) is required for flagellar adhesion-mediated mating (Huang *et al.*, 2007). RNAi knockdown of CrPKD2 does not interfere with flagellar adhesion between the (+) and (−) gametes, but does block downstream signaling, resulting in the reduction of gamete fusion and formation of diploid cells (Huang *et al.*, 2007). Studies have shown that, in this pathway, CrPKD2 functions downstream of flagellar adhesion but upstream of a flagellar protein tyrosine kinase, which leads to downstream activation of the cGMP-dependent protein kinase CrPKG (Wang *et al.*, 2006) and an adenylate cyclase that produces cAMP (Wang and Snell, 2003). cAMP appears to be the critical second messenger because exogenously supplied cAMP is sufficient to induce gamete fusion, bypassing the steps of CrPKD2, CrPKG, and the adenylate cyclase. CrPKD2 is also present in flagella of vegetative cells, and so it is likely to have additional functions in other signaling pathways, possibly including control of flagellar motility (Huang *et al.*, 2007).

The *Drosophila* Pkd2 is highly enriched on the sperm flagellum (Gao *et al.*, 2003), and its expression in S2 *Drosophila* tissue culture cells generates cation channel activities similar to those of mammalian PKD2 (Venglarik *et al.*, 2004). As a normal reproductive process, *Drosophila* sperm in the uterus travel into a long and narrow seminal receptacle (SR) tubule that has a closed end. Sperm are stored in the distal half of the SR for weeks, and during this period, they gradually exit out of the SR to fertilize the egg (Bloch Qazi and Wolfner, 2006). Mutant sperm lacking wild-type *Pkd2* show grossly normal motility but are unable to move efficiently into the SR (Watnick *et al.*, 2003; Gao *et al.*, 2004). This leads to a working model that *Drosophila* sperm storage is induced by an SR entry signal that activates Pkd2, leading to calcium influx into the sperm and thereby producing the specific swimming behavior necessary for SR entry. Here, we report the identification of CG34110, another flagellar protein required for the *Drosophila* sperm to enter the SR tubule. Loss-of-function *CG34110* results in specific sperm motility defects that are essentially the same as those of the *Pkd2* mutant. CG34110 has unequivocal orthologues in organisms possessing motile cilia and flagella, but is absent in organisms that do not have cilia and in *C. elegans*, which does not have motile cilia. Biochemical analyses indicate that the *C. reinhardtii* orthologue FAP50 (Pazour *et al.*, 2005) is an OD-associated protein unaffected in all three *mbo* mutants.

RESULTS

lobo is a new locus required for sperm storage

There are two types of sperm storage organs in female *Drosophila*: one coiled SR tubule and two mushroom-shaped spermathecae (Figure 1A). We initially identified a recessive storage-defective mutation and mapped its meiotic position to ~990 kb distal to a P element insertion *P(XP)kal-1*^{d01966}. The P element insertion was removed by recombination, resulting in a "clean" storage-defective locus named *lost boys* (*lobo*) (see *Materials and Methods*). The wild-type sperm entered the storage organs (Figure 1B), whereas few sperm from the *lobo* homozygous males entered the storage organs (Figure 1C). This phenotype is similar to the characterized

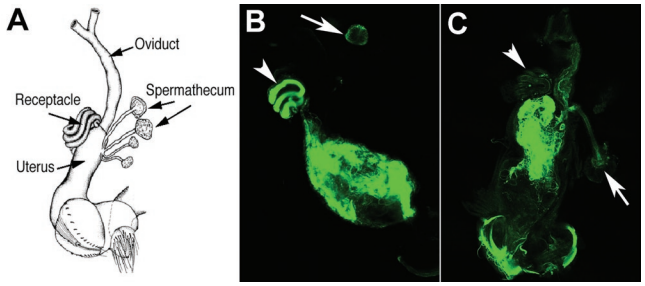

FIGURE 1: The sperm storage phenotype of *lobo*. (A) A schematic diagram of the female reproductive tract. (B, C) Confocal images of freshly dissected uteri from wild-type females at 30 min after mating with the wild-type (B) and *CG34110^{lobo}* homozygous males (C). Both types of sperm were transferred into the uteri as indicated by the green fluorescence derived from the reporter transgene *dj-GFP* that labels the sperm flagellum. The mating plug is located at the posterior uterus, where it lacked the GFP fluorescence. The wild-type sperm entered the SR (arrowhead) and spermatheca (arrow), whereas very few of the mutant sperm entered the two storage organs. Low levels of auto-fluorescence were present in the fly tissue.

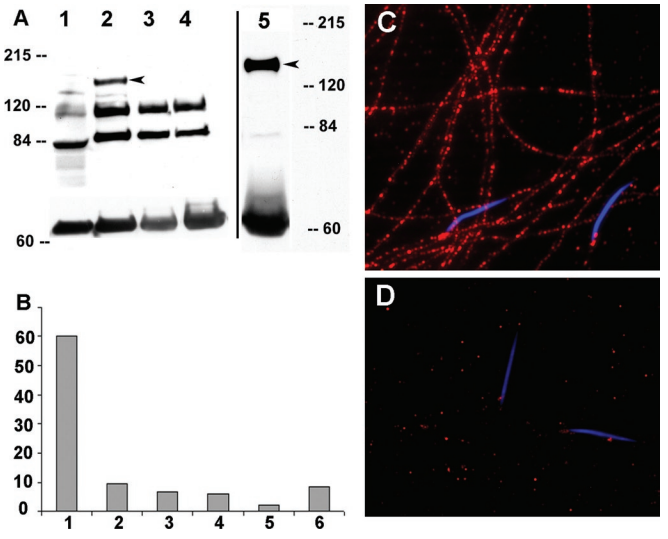

FIGURE 2: Western blot, male fertility, and CG34110 immunofluorescence staining. (A) The CG34110 protein was detected by either anti-CG34110$^{861–874}$ or anti-CG34110$^{828–842}$ as a band running at ~167 kDa (arrowhead) on the Western blot. Protein samples were from adult wild-type females (lane 1); wild-type testes (lane 2); mutant testes from *CG34110^{lobo}* (lane 3); and *CG34110^{MB00722}* (lane 4) and wild-type mature sperm from the male SV (lane 5). The band near 60 kDa was α-tubulin detected by mouse anti–α-tubulin (Sigma DM1A) as a loading control. Two other bands were likely nonspecific bands that were strong in the testis but undetectable in the mature sperm. (B) Male fertility was measured as the average number of F_1 progeny (*y* axis) produced during the first 48 h by one wild-type female following mating with one male of different genotypes (*x* axis). The male genotypes are as follows: 1) wild type (F_1 = 60, n = 10), 2) *CG34110^{lobo}* (F_1 = 9.6, n = 12), 3) *CG34110^{lobo}/Df(3R)Exel6201*, (F_1 = 6.5, n = 11), 4) *CG34110^{Q46}/Df(3R)Exel6201* (F_1 = 6.1, n = 10), 5) *CG34110^{MB00722}/Df(3R)Exel6201* (F_1 = 2.2, n = 24), and 6) *CG34110^{MB00722}/CG34110^{lobo}* (F_1 = 8.7, n = 10). (C, D) Mature sperm were collected from the male SVs and stained with the anti-CG34110 antibody. The immunoreactivity (red) was observed along the entire sperm tail from wild type (C) but not in sperm from the mutant male (D; *CG34110^{MB00722}/CG34110^{lobo}*). The DNA of the sperm heads was stained blue by DAPI.

phenotype of *Pkd2* on the second chromosome. The *lobo* locus is clearly a distinct locus because it is on the right arm of the third chromosome (3R).

To identify the responsible gene, genetic complementation tests were carried out between *lobo* and genomic deletions distal to *P(XP)kal-1^{d01966}*. The *lobo* locus was found to fall within the *Df(3R) Exel6201* deletion but outside of the distal flanking deletion *Df(3R) Exel9056*. This suggested that the responsible gene lies within the 59 kb of DNA at coordinates 3R:20963561..21022720. To verify the deletion breakpoints, the (*deletion*/+) DNA samples were isolated and used to hybridize to long oligonucleotide microarrays and compared with (+/+) DNA samples in parallel. The microarray data indicated that *Df(3R)Exel9056* did not obviously delete any genes, whereas *Df(3R)Exel6201* deleted five annotated genes (*CG13652*, *CG13651*, *CG34110*, *CG13653*, and *CG11849*); only one of these, *CG34110*, is highly expressed in the male testis (Chintapalli *et al.*, 2007).

Consistent with *CG34110* being the responsible gene, *lobo* failed to complement *CG34110^{MB00722}*, which contains a Minos transposon insertion. Excision of *CG34110^{MB00722}*, via Minos transposase-induced transposon excision (Metaxakis *et al.*, 2005), led to a reversion of the phenotype back to wild type, suggesting that the Minos insertion was causing the storage defect. DNA sequencing indicated that the Minos transposon inserts at $E^{378}\downarrow Y^{379}$ (GTTGT↓ACTCA) and produces a 378-amino-acid (aa) truncated polypeptide of the full-length CG34110 protein of 897 aa. In addition, *lobo* is a 7-base pairs (bp) deletion (ctgcact) in exon 6 of *CG34110*, which produces a 567-aa truncated polypeptide. Thus *lobo* is referred to as *CG34110^{lobo}*.

To further verify that *CG34110* is the responsible gene, antipeptide antibodies were produced and targeted to recognize two nonoverlapping regions of CG34110. Both antibodies were found to bind to a protein of ~167 kDa (arrowhead in Figure 2A) on Western blots of protein samples derived from wild-type testis (Figure 2A, lane 2) and mature sperm (Figure 2A, lane 5). The band was not detectable in samples from wild-type adult females (Figure 2A, lane 1) and testes from *CG34110^{lobo}* or *CG34110^{MB00722}* homozygous males (Figure 2A, lanes 3 and 4). During the course of this study, we isolated the *CG34110^{Q46}* allele by chemical mutagenesis in an F_3 genetic screen. Thus the *CG34110* locus is defined by three independently derived loss-of-function alleles (*Q46*, *lobo*, *MB00722*) with severity close to that of the gene deletion *Df(3R) Exel6201* (Figure 2B).

CG34110 is a highly conserved flagellar protein

A reduction of sperm storage could be caused by a defect in the sperm or a defect in the seminal fluid proteins that are known to influence the efficiency of sperm storage (Neubaum and Wolfner, 1999). To localize CG34110 expression, immunostaining was done with the male reproductive tract, including the accessory gland and ejaculatory duct (ED), but only the testis and sperm showed positive protein staining. As all sperm proteins are produced during spermatogenesis in the testis, CG34110 is likely to assemble and function in the sperm, which is supported by CG34110 immunofluorescence along the sperm flagellum (Figure 2C). The CG34110 staining appears as regular puncta along the flagellum; based on the 9-μm sperm head in the same image, the periodicity of the puncta is ~10× greater than that of the 96-nm repeats of inner dynein arm complexes along the axoneme (Piperno *et al.*, 1990).

To define the extent of functional conservation, Blastp searches were conducted and showed that, with a probability value of 2e-70

to 6e-78, CG34110 has an unequivocal vertebrate orthologue Ccdc135 (synonymous with Gm770 [McClintock *et al.*, 2008], SRG-L, and SRG-S [Guo *et al.*, 2004; Ma *et al.*, 2006]). Ccdc135 is conserved in human, mouse, rat, chicken, and zebrafish, but not *C. elegans*, rice, and *Arabidopsis*. The alignment between CG34110 and Ccdc135 shows extensive sequence conservation throughout the entire polypeptide (~29% identity, ~46% similarity, Supplemental Figure 1). Expression report from Unigene (http://www.ncbi.nlm.nih.gov/unigene) indicates that Ccdc135 is highly expressed in the nasopharynx, which includes respiratory epithelial cells with motile cilia, and in the testis. Gm770 was previously predicted to have a high probability of ciliary function based on differential expression in tissues containing motile cilia (McClintock *et al.*, 2008).

Ccdc135 was predicted by others (Ma *et al.*, 2006) to contain a transmembrane domain and possibly enzymatic activity. These features, however, could not be confirmed upon careful inspection of Ccdc135 or CG34110. Protein domain searches were carried out with current programs on the ExPASy Proteomics Server. CG34110 does not contain recognizable calcium- or calmodulin-binding motifs. The only protein structural features we could identify are four regions (aa153–173, aa436–460, aa633–652, and aa787–807; Supplemental Figure 2) that each contain three heptad repeats. Such heptad repeats with apolar residues separated alternately by three and four residues are frequently involved in the formation of alpha-helical coiled coils or alpha-helical bundles (Parry *et al.*, 2008). In this case, the repeats lack oppositely charged residues in positions necessary for forming interchain ionic interactions that are often seen with two- and three-stranded coiled coils. This indicates a greater probability of forming alpha-helical bundles, probably four-stranded for CG34110, rather than a coiled coil structure.

FAP50 is associated with the outer doublets

Blast searches indicate that CG34110 is a mutual best fit to a *C. reinhardtii* flagellar-associated protein, FAP50, that was identified by more than 30 peptide hits in the published *C. reinhardtii* flagellar proteome (Pazour *et al.*, 2005). The peptides from FAP50 were found exclusively in fractions derived from the axoneme, suggesting that FAP50 is an axonemal component. To confirm this and to locate FAP50 more precisely within the axoneme, we made a peptide antibody to FAP50. The antibody reacted with three bands in Western blots of isolated flagella, one of which (Figure 3A, arrowhead) is in the region of the gel from which virtually all of the FAP50 peptides originated in the proteomic analysis (Pazour *et al.*, 2005). This protein was highly enriched in flagella versus whole cells (Figure 3B), indicating that FAP50 is likely to function specifically in the flagellum. In Western blots of flagellar fractions (Figure 3B), FAP50 was found almost exclusively in the 0.6 M KCl-extracted axonemes (EX-AX, contains primarily ODs, including radial spokes but lacking most dynein arms), was not detectable in the NP-40-soluble membrane-plus-matrix fraction (M+M, contains flagellar membrane proteins, intraflagellar transport proteins, and other soluble proteins of the flagellar matrix), and was barely detectable in the 0.6 M KCl extract (KCL-EX, contains inner and outer dynein arms and many CP proteins). Extraction of the axoneme by 0.6 M KCl solubilizes almost all outer dynein arms and substantial amounts of most inner dynein arm components (Pfister *et al.*, 1982; King *et al.*, 1986; Kagami and Kamiya, 1990, 1992; Pazour *et al.*, 2005; Yagi *et al.*, 2009) (Supplemental Table 2). Therefore FAP50 appears to be specifically associated with the ODs but not with their dynein arms. This is consistent with a previous result that FAP50 is present in the flagellar axoneme of a mutant lacking the outer dynein arms (Pazour *et al.*, 2005). To learn more about the location of FAP50 within the axoneme, we compared isolated flagella of wild type, the mutant *pf18* which lacks the CP, and the mutant *pf14* which lacks the radial spokes. FAP50 was present at wild-type levels in the flagella of both *pf18* and *pf14* mutants (Figure 3C). Therefore FAP50 is a component of the ODs but appears not to be a subunit of the dynein arms, the radial spokes, or the CP.

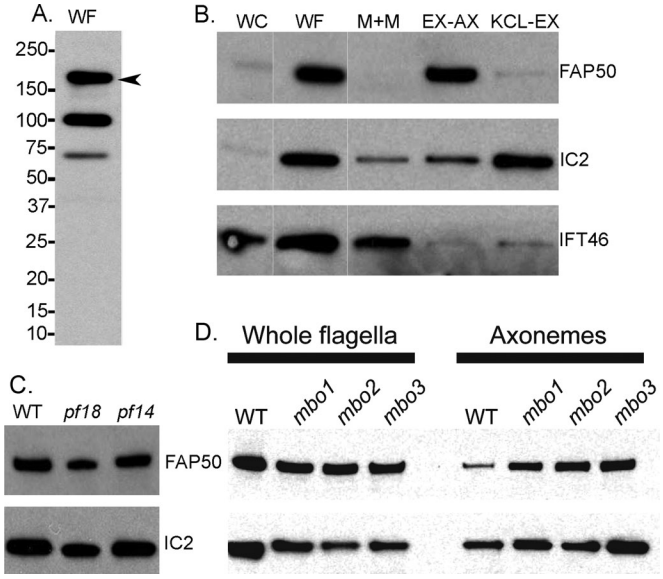

FIGURE 3: Association of *C. reinhardtii* FAP50 with the ODs. Western blots of *C. reinhardtii* isolated whole flagella (WF), whole cells (WC), the 1% NP-40-soluble flagellar membrane-plus-matrix fraction (M+M), the axonemal fraction remaining after extraction with 0.6 M KCl (EX-AX), and the 0.6 M KCl extract (KCL-EX). (A) Anti-FAP50 detected three bands in WF, one of which (arrowhead) is FAP50 based on the gel region that yielded FAP50 peptides in the flagellar proteomic analysis (Pazour *et al.*, 2005). (B) The first two lanes were loaded at a ratio of 1 cell-to-2 flagella; lanes 2–5 were loaded with protein from equivalent numbers of flagella. Blots were probed with antibodies to FAP50 (1:4000 dilution), and to the outer dynein arm intermediate chain IC2 and the intraflagellar transport protein IFT46 to verify purity and correct loading of the fractions. Thin, white, vertical lines indicate where marker lanes were excised from the image. (C) Whole flagella from wild type (WT), the CP-less mutant *pf18*, and the radial spoke-less mutant *pf14* were probed with antibodies to FAP50 and to IC2 as a loading control. (D) Isolated flagella or axonemes (obtained after 1% NP-40 treatment) from WT and the three *mbo* mutants were probed with anti-FAP50 and anti-IC2.

In *C. reinhardtii*, three independent mutations (*mbo1*, *mbo2*, and *mbo3*) result in a phenotype in which the flagella propagate only the symmetrical waveform used for backward swimming and are unable to form the asymmetrical waveform used for forward swimming (Segal *et al.*, 1984). The *mbo* mutant flagella lack six to eight proteins normally present in wild-type flagella. The mutations also correlate with loss of a beak-like projection in the lumens of a subset of the ODs. Because the proteins missing in the *mbo* mutants are involved in waveform control and may be localized to the ODs, we investigated whether FAP50 is defective in these mutants. All three *mbo* mutants had normal levels of FAP50 (Figure 3D), indicating that FAP50 is not one of the constellation of six to eight proteins associated with the move-backward-only phenotype.

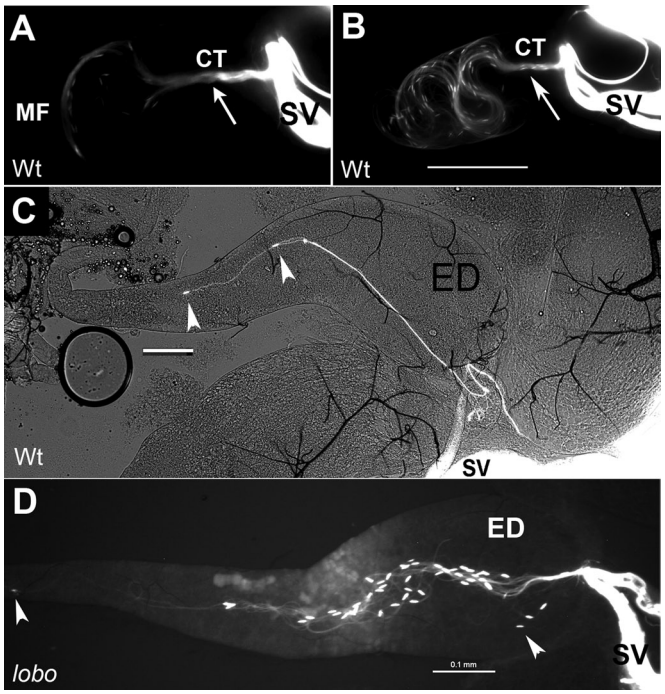

FIGURE 4: Movement of sperm from the SV into the ED in the male. The sperm heads and tails were marked with GFP, and the images were obtained by GFP imaging. (A, B) Video snap views from Supplemental Movie 1, which captured sequential events occurring in the reproductive tract of a wild-type male within 1–4 min following its copulation with a wild-type female. The sperm exited out of the bilateral SV through a converging tubule (CT, arrow) and entered the ED. Sperm heads were visible as GFP specks (arrowheads) at the leading edges of the moving front (MF). (C, D) Still images obtained from fast-freezing copulating wild-type (C) and *lobo* mutant males (D, $CG34110^{MB00722}/CG34110^{lobo}$). Scale bars are all 0.1 mm.

lobo does not affect sperm exit movement from the seminal vesicle

To elucidate the function of *CG34110* and compare its mutant phenotype with that of the *Pkd2* mutant, sperm heads and tails were marked with *Protamine-GFP* and *Dj-GFP* transgenes (Santel *et al.*, 1997; Rathke *et al.*, 2007), and movement was examined by fluorescence microscopy. During copulation, the male and female reproductive tracts join together, forming a continuous conduit for the sperm to travel from the male into the female. The first narrow tubule in the sperm conduit connects the bilateral male seminal vesicles (SVs), where mature sperm are stored, to the outgoing ED. Shortly after mating commences, the exit tubules of the SVs open and sperm heads (short specks, arrowheads in Figure 4) lead the way out of the SVs through a connecting tubule (CT; Figure 4A) and enter the ED (Supplemental Movie 1). Because the ED (its distal end is broken off in Figure 4C) has a length similar to that of the sperm, the sperm heads captured in Figure 4 are leading ends of the sperm. Approximately 200 sperm heads passed through the CT to enter the ED while the sperm moving front (MF) advanced up to the anterior ~1/8 of the ED length (Figure 4B); the tail ends of these sperm have not entered the ED at this time based on length measurement of the flagellar portion that was inside the ED.

To confirm the head-leading orientation, the coupling flies were fast-frozen and the male ED was imaged (Figure 4, C and D). These still images validated the video observation and provided numerical data that 96% (n = 215) of the wild-type sperm found in the ED have the head-leading orientation. The mutant alleles analyzed ($Pkd2^{ko67}$ [Gao *et al.*, 2004], $Pkd2^{1}$ [Watnick *et al.*, 2003], $CG34110^{MB0072}$, and $CG34110^{lobo}$) are near complete loss-of-function mutations with little residual male fertility (Figure 2B). The majority of the *Pkd2* mutant sperm (96% for $Pkd2^{ko67/1}$, n = 103; 96% for $Pkd2^{ko67/KO67}$, n = 68; 98% for $Pkd2^{ko67}/Df(2L)prd1.7$ n = 116) and the *lobo* mutant sperm (98% for $CG34110^{lobo/MB00722}$, n = 257) also exited the CT with head-leading orientation (Figure 4D). Consistent with this, the amount of sperm inseminated into the uterus is similar for wild-type, *Pkd2*, and *lobo* males (Figure 1) (Gao *et al.*, 2003; Watnick *et al.*, 2003).

lobo affects sperm entry movement into the female seminal receptacle

In the uterus, flagella of wild-type sperm move with circular-shaped bends and the sperm head is dragged behind the flagellum (Figure 5A and Supplemental Movie 2). From the uterus, ~5-10% of the wild-type sperm enter the female SR tubule (an average of 330 sperm out of 4000–6000 in the ejaculate; Supplemental Table 1). The maximum number of sperm in the SR was reported to be 400 (Manier *et al.*, 2010). The proximal half SR (PSR; 1 mm long, ~19 μm wide) is slightly narrower than the distal half SR (DSR; 1 mm long, ~24 μm wide). The PSR serves as the passageway for the sperm to go in or out of the DSR, whereas the DSR is the site of sperm storage (Figure 5, J and K). Wild-type sperm pass through the PSR in bundles (Figure 5B), as shown by the exposed parallel sperm flagella at the region where the PSR tubular wall was teased open (Figure 5C). The sperm in the exposed flagellar bundles have a tail-leading orientation (Figure 5C, arrowheads). To determine the initial sperm entry orientation, still images were obtained from copulating flies that were fast-frozen at an early stage of sperm storage (15 min from mating onset), and the orientations of individual sperm that had entered the PSR were observed. The tail end of the wild-type sperm was found to enter the PSR first (Figure 5D), and the sperm went through the PSR tubule without making turns (Supplemental Movie 3). Quantification showed that the tail-leading orientation occurred at a frequency of 80% (20/25 sperm), whereas the head-leading orientation (2/25 sperm) and flagella with one hairpin-shaped fold (3/25 sperm, similar to Figure 5F) were found in only a minority of the sperm. The explanation for the minority head-leading and folded sperm is uncertain, but they may represent transitional forms of sperm during their normal conversion from the folded form in the uterus to the extended parallel form at the initiation of PSR entry (see *Discussion*).

In contrast to wild-type sperm, the *lobo* mutant sperm ($CG34110^{MB00722/lobo}$) show increased frequencies of head-leading orientation during PSR entry and excessive flagellar folding in the PSR lumen. Still images were obtained for the *lobo* mutant in the same manner as for wild type. This showed that the head-leading entry orientation was increased from the 8% wild-type baseline to 55% (18/33 sperm) for the *lobo* mutant such that multiple *lobo* mutant sperm heads were found to enter the PSR simultaneously (Figure 5E), which was not observed for wild-type sperm. In addition, the folded flagellar configuration was increased from the 12% wild-type baseline to 24% (8/33 sperm) for the *lobo* mutant. Although flagella with one hairpin-like fold (similar to Figure 5F) were occasionally observed for the wild-type sperm, only the mutant sperm showed excessive folding into tangles (Figure 5G). Many tangled flagella were found in freshly dissected PSRs at later hours when sperm storage had stopped as indicated by the extrusion of inseminated sperm out of the uterus. This suggests that the tangled flagella were trapped in the PSR and unable to move into the DSR. The

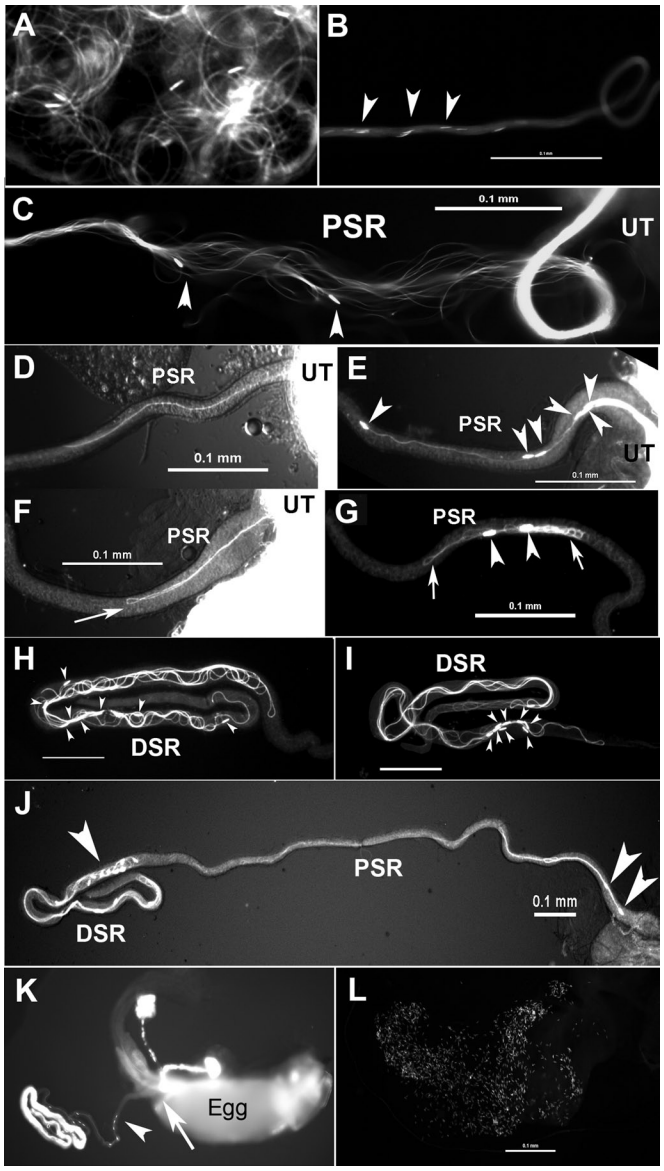

FIGURE 5: Sperm transitory movements in between different compartments of the female reproductive tract. These images were obtained by imaging sperm labeled with head (short specks, arrowheads) and tail GFP. Sperm are wild type in (A–D, K); $CG34110^{MB00722}/CG34110^{lobo}$ in (E, F, G, J); $Pkd2^{KO67}/Pkd2^{KO67}$ in (H, I); and the *Pkd2 lobo* double mutant in (L). (A) A video snap view of moving sperm inside the uterus (Supplemental Movie 2). The flagella were propagating circular-shaped bends and the heads were dragged by their flagella during the movement. (B–J) Various segments of the PSR or DSR with the uterus (UT) positioned on the right and the DSR on the left. (B) A section of the PSR tubule is shown with its lumen filled with wild-type sperm flagella and the heads are visible along its length. (C) When the tubular wall was teased open at a central point of the PSR, it revealed a parallel bundle of sperm inside the lumen. Arrowheads point to two heads that were apparently in tail-leading orientation toward the DSR on the left. (D) The tail end of a wild-type sperm entered the PSR first. (E) In contrast, the heads of multiple *lobo* mutant sperm entered the PSR first, as did *Pkd2* mutant sperm (not shown). (F) A *lobo* mutant sperm flagellum formed a hairpin-shaped fold (arrow) in the PSR lumen. (G) Two *lobo* mutant sperm became folded into large tangles, as did flagella of *Pkd2* mutant sperm (not shown). Such tangles were still present in the PSR after the bulk sperm was extruded out of the UT, suggesting that they were stuck. (H) After entering the DSR, the wild-type, *Pkd2*, and *lobo* mutant sperm were similarly folded with heads distributed at random positions, as shown here for the *Pkd2* mutant sperm. (I) In some images, the sperm heads in the DSR were found to reorient toward the UT, as if they were ready for DSR exit. (J) Many *lobo* sperm in the DSR had their heads oriented toward the UT, and two of the *lobo* sperm were returning to the UT with a head-leading orientation, just like the wild-type sperm in (K). (K) The reproductive tract of an egg-laying wild-type female following mating with a wild-type male. The egg is large enough to occupy the entire uterus and the sperm entry point on the egg shell, the micropyle (arrow), faces the openings of the storage organs. The arrowhead points to a group of head-leading sperm in the PSR that leads to the egg (see larger version of the image in Supplemental Figure 3). (L) The uterus from a female after mating with the double-mutant male ($Pkd2^{ko67/MB06703}$; $CG34110^{MB00722/lobo}$) contained a large number of sperm (only heads are visible with the head GFP marker). Scale bars are all 0.1 mm.

remainder of the *lobo* mutant sperm at the proximal end of the PSR were in tail-leading orientation, although the frequency was reduced from the 80% wild-type level to 21% (7/33 sperm). Similar to the *lobo* mutant, the *Pkd2* mutant sperm ($Pkd2^{ko67/1}$) also show increased head-leading entry orientation and excessive flagellar folding in the PSR lumen (30% head-leading, 55% folded flagellum,15% tail-leading, n = 84). At later time points (1–4 h after mating), the phenotypes of both the *Pkd2* and *lobo* mutant sperm were more severe, with mostly tangled flagella in the PSR lumen (similar to Figure 5G), and the number of mutant sperm that entered the DSR was reduced by 100-fold (Figure 6). These observations suggest that initial deviations from wild-type flagellar configuration at the PSR entry reflect the underlying motility defects of the mutant sperm that, over the duration of PSR passage, lead to a severe reduction of sperm storage.

Comparisons of *Pkd2* and *lobo* single mutants with the double mutant

To determine possible differences between *Pkd2* and *lobo*, the numbers of sperm that entered the DSR were determined for *Pkd2* and *lobo* single mutants and the double mutant. Like the single mutants, the double-mutant male produced a large number of motile sperm that entered the uterus (Figure 5L), suggesting that motility required for sperm transfer from male to female was grossly normal. In contrast to wild-type males, which consistently lead to ~275–404 sperm in the DSR (Supplemental Table 1), the numbers of the mutant sperm that enter the DSR varied greatly on an individual basis, from male to male or from one mating to the next mating of the same male. The overall storage patterns were determined by examining 100–150 individual males (Figure 6). The percentages for each storage class are zero sperm (30.1%), 1–5 sperm (55.3%), 6–10 sperm (9.7%), 11–15 sperm (2.9%), and 16–20 sperm (1.9%) for $Pkd2^{KO67/KO67}$ (average 2.8 sperm stored per female per mating [sp/f/m]). Similar patterns were observed for $Pkd2^{ko67/MB06703}$ (average 5.5 sp/f/m), $CG34110^{MB00722/lobo}$ (average 4.0 sp/f/m), and the double mutant ($Pkd2^{ko67/MB06703}$; $CG34110^{MB00722/lobo}$, average 2.4 sp/f/m), with the highest numbers of sperm stored to be 21, 22, and 24 for the respective genotypes (Figure 6). These patterns of sperm storage suggest that successful entrance into the DSR is stochastic. Possibly, the mutant sperm enter the DSR if they, by chance, do not get stuck in the PSR lumen. Although the double mutant showed a more severe phenotype than either of the single mutants in the combination, the differences were very small (~3 sperm or ~1% of the wild-type average of 330 sperm). Such small differences are normally observed for males of different genetic backgrounds

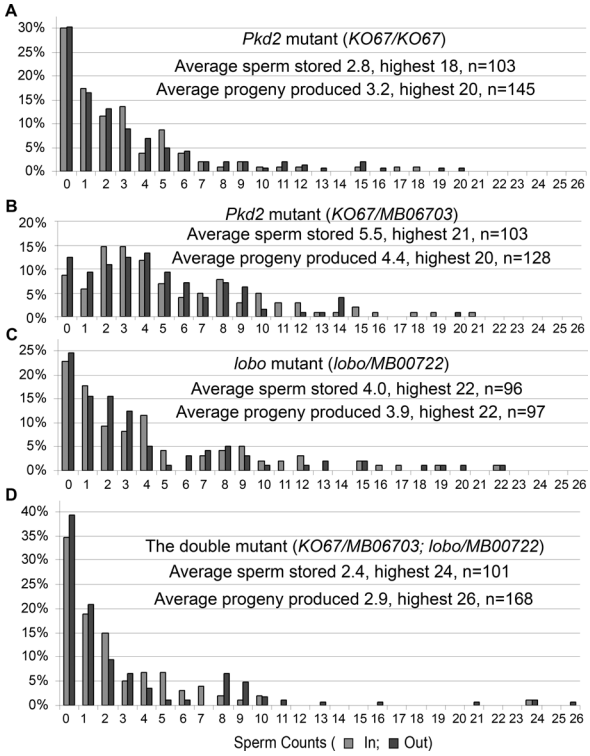

FIGURE 6: Comparison of sperm counts in the DSR with the progeny produced for the *Pkd2* and *lobo* single mutants and the double mutant. The *x* axis indicates sperm counts; "In" for the number of sperm stored in the DSR per female per mating and "Out" for the number of viable F_1 progeny produced per female per mating. Each data point was obtained from one wild-type female (collected as virgin) after mating with one mutant male. The four male mutant genotypes are (A) $Pkd2^{Ko67}$, (B) $Pkd2^{Ko67/MB06703}$, (C) $CG34110^{lobo/MB00722}$, and (D) $Pkd2^{Ko67/MB06703}$; $CG34110^{lobo/MB00722}$ (also carrying one copy of *Protamine-GFP*). The *y* axis represents the percentages of the "In" or "Out" in the tested populations (n). All progeny were checked for the expected genotype to make sure that they were fathered by the experimental males. The wild-type male consistently stores an average of 330 sperm (range 275–404, Supplemental Table1).

(Gao *et al.*, 2003) and for males with or without the *Protamine-GFP* transgene (Figure 2B vs. Figure 6). Green fluorescent protein (GFP) expression in the sperm by itself does not alter the overall functionality of the sperm, although it does cause some variability in sperm fitness assays (Manier *et al.*, 2010).

After entering the DSR, the single- and double-mutant sperm were all motile, and the swimming speed of the double mutant was not obviously different from that of wild type (Supplemental Movies 4 and 5). The stored sperm exit through the same PSR passageway for fertilization. To determine whether the motility required for fertilizing the egg was affected, the number of F_1 progeny produced was compared with the number of sperm stored. As shown in Figure 6, the overall patterns of F_1 progeny produced were in striking agreement with the patterns of sperm storage for the single- and double-mutant males. T-test does not indicate discrepancy between the numbers of sperm stored and the numbers of F_1 progeny produced within each genotype.

Drosophila sperm enter the egg through a small micropyle opening on the egg shell (arrow in Figure 5K). As the egg descends from the ovary into the uterus, the micropyle faces the openings of the storage organs (Figure 5K) (Snook and Karr, 1998). The egg-laying process results in the extrusion of unstored sperm out of the uterus (Figure 5K). Aside from egg laying, a recent study showed that the unstored sperm are ejected out of the uterus before the first egg is laid and 84% of the females no longer contain unstored sperm 5 h after mating (Manier *et al.*, 2010). To determine whether the stored double-mutant sperm could exit the DSR and fertilize the egg, we did time-course counts of the F_1 progeny produced. When wild-type females were mated with the double-mutant males, the eggs laid in the first 6 h after mating accounted for 0–6.8% of the total F_1 progeny produced, leading to the possibility that as many as 93% of the F_1 progeny could be fertilized by the double-mutant sperm that entered the DSR. We also examined F_1 production by the females that had already laid eggs. At 8 h after mating, many mated females (n = 30) had laid 1–12 fertilized eggs (n = 113 F_1); these females were found to produce an additional 91 progeny afterward (45% of the total F_1 produced). The females that had already laid 4–12 eggs were found to produce an additional 2–9 F_1 progeny that were fertilized by the double-mutant sperm.

We also examined the movement orientation of the sperm that exit the PSR by imaging the PSRs obtained from females fast-frozen at 24 h after mating. Wild-type sperm travel out of the PSR with a head-leading orientation (Figure 5K; head-leading in 30/30 sperm). The *lobo* mutant sperm also showed head-leading orientation (Figure 5J; head-leading in 23/24; tangled flagella in 1/24). Many *Drosophila* species have long sperm; while their heads enter the egg, their tail tips hang outside of the egg shell in at least four species analyzed, including *D. melanogaster* (Karr and Pitnick, 1996). Thus the head-leading SR exit orientation that we observed probably readies the sperm for a head-in-first fertilization of the egg.

DISCUSSION

This study reports a novel motility function for the conserved flagellar protein CG34110/Ccdc135/FAP50 through genetic analysis of a *Drosophila* sperm storage–defective mutation *lobo*, which encodes CG34110. The study encompasses the initial genetic screen for *lobo*, molecular identification of the culprit gene, and detailed motility analyses that show that the *Pkd2* and *lobo* single mutants and the double-mutant sperm have essentially the same motility phenotypes. The biochemical analyses presented here together with the published flagellar proteomic study clearly demonstrate that the *C. reinhardtii* orthologue FAP50 (Pazour *et al*, 2005) is associated with ODs of the flagellar axoneme. In a Clustal analysis of the proteome data, FAP50 grouped closely with many OD-associated proteins (Pazour *et al.*, 2005), including RIB43a, a component of the tektin ribbon filament on the ODs (Norrander *et al.*, 2000). This is consistent with Western blot results of normal FAP50 abundance in *C. reinhardtii* mutant flagella lacking the CP and radial spoke structures. Furthermore FAP50 protein levels on the axoneme were unaffected by 0.6 KCl extraction that removes almost all outer and inner dynein arm components and unaffected in flagella of three *C. reinhardtii* mutant strains (*mbo1*, *mbo2*, *mbo3*) that lack axonemal proteins required for the formation of asymmetrical flagellar bends. Therefore FAP50 may represent a novel regulatory protein located on the OD microtubules of the axoneme.

A second intriguing finding is that the fly sperm appears to move with either head- or tail-leading orientation. The majority of sperm exit the SV with a head-leading orientation (Supplemental Movie 1), whereas the majority of sperm in the uterus move with the head dragging behind the flagellum (Supplemental Movie 2). Such an ability to move in both axial directions has only been shown in a few organisms (see *Introduction*), but this is not unexpected for

superlong sperm that have to move within the narrow confines of the male or female reproductive tract. Sperm movement is powered by bending of the flagellum. The flagellar bends push against the surrounding medium, thereby generating the force for forward movement. When a symmetrically bending flagellum switches to asymmetrical bends, this effectively alters the vector of the force generated. This is how most types of sperm make turns during chemotaxis or obstacle avoidance. However, because the fly sperm is as long as the SR tubule and the tubule has a length-to-width ratio of 100:1, asymmetric flagellar bending would unlikely be effective in the narrow confines of the SR tubule. The acquisition of bidirectional movement capability by the *Drosophila* sperm could be an adaptation of the long sperm to the narrow tubular structures of the reproductive tract since this provides an alternative strategy for backing up and obstacle avoidance. It would be interesting to determine whether long sperm in other insect species have evolved bidirectional movement capability. Interadaptive changes between the sperm and the female SR have been shown in experiments where selection for females with longer SRs results in longer sperm in the selection population in as little as 30–40 generations (Miller and Pitnick, 2002).

It is interesting that the fly sperm seems to adopt preferentially one of the two possible orientations for specific movements within the reproductive tract. This is also an expected finding because, if bidirectional movements are not tightly regulated, it would lead to frequent directional reversal and the sperm would end up staying at the same place. Due to the large number of sperm in the reproductive tract, we cannot be sure that each and every individual sperm is moving with one orientation at a given time or condition. However, this does not present a critical issue because, having a bidirectional movement capability, the sperm is likely to be able to reverse its movement orientation when situations call for it. In trypanosomes, which also have a bidirectional movement capability, basal levels of orientation reversal are observed in the absence of encounters with obstacles (Sugrue *et al.*, 1988). To our knowledge, absolute uniformity of sperm behavior is difficult to find and variability occurs in many situations. Sperm motility is known to vary depending on sperm maturation and competency (Immler, 2008; Werner and Simmons, 2008). A general phenomenon related to sperm in a variety of chemotaxis settings is that only a small fraction (usually <10% of the sperm) responds to physiological signals (reviewed in Kaupp *et al.*, 2008; Eisenbach and Giojalas, 2006). We determined that 5–10% of the sperm in the uterus enter the DSR. The sperm in the uterus are moving with circularly bending flagella (Figure 5A), whereas sperm moving within the PSR lumen are mostly parallel to each other (Figure 5C). The PSR-entry-responding sperm from the crowded sperm mass in the uterus may carry along the nonresponding sperm that are folded, leading to our observation of some sperm that are folded or have a head-leading orientation at the PSR opening. Some of the folded flagella we saw in the PSR could correspond to sperm in normal transition from the folded to the extended parallel form according to a working model of *Drosophila* sperm storage (Yang and Lu, 2011). As shown in Supplemental Movie 3, the wild-type sperm can go all the way through the PSR to enter the DSR without making any turns. This is at least one of the modes that the sperm move into the DSR.

In a previous study, gross sperm motility such as beat frequency was not obviously affected in the *Pkd2* mutant sperm that were taken out of the male SV and analyzed in vitro (Watnick *et al.*, 2003). To elucidate the *Pkd2* and *lobo* motility function, here we took an in vivo approach. The data showed that *Pkd2* and *lobo* single mutants and the double mutant exhibit essentially the same spectrum of phenotypes. The motility required for the sperm to enter the SR tubule is severely impaired, whereas the motility required for sperm transfer from male to female is grossly normal. Both the single- and double-mutant males can father viable progeny to a degree comparable to the number of mutant sperm that enter the DSR, suggesting that the motility required for fertilization is unlikely to be affected. The observed differential motility effect is likely to reflect the true functions of *Pkd2* and *CG34110* because the analyzed mutant alleles exhibit phenotypic severity close to that of gene deletions. Based on the established flagellar propulsion theory and hydrodynamic principles (Brokaw, 2006), the bidirectional sperm movement is the consequence of flagellar wave propagation in either base-to-tip or tip-to-base direction. The folded or parallel flagellar configuration reflects the waveform the sperm is propagating. Our analyses suggest that successful sperm storage requires a waveform compatible with forming linear arrays of flagellar bundles, and it also requires preferential wave propagation from one of the ends (in this case, the tail end) so that the sperm can travel into the DSR. Without wild-type Pkd2 or CG34110 activity, the mutant sperm enter the PSR with the wrong or random orientation, and the sperm tend to be trapped in the lumen with abnormal flagellar folding. These phenotypes could be interpreted as failure of waveform conversion and inappropriate switching between head-leading and tail-leading swimming modes. Waveform conversion and regulation of wave propagation could be two aspects of a single process that is regulated by Pkd2 and CG34110.

Currently, very little is known about how the direction of flagellar wave propagation is controlled, yet this is important for all flagella because an unstable direction of wave propagation would result in unproductive locomotion. Our characterization of in vivo sperm behavior in *Drosophila* and the roles of *Pkd2* and *CG34110* provide a new opportunity to address mechanisms of wave propagation and waveform conversion. Furthermore, CG34110 has highly conserved orthologues in species containing motile cilia, but homologous genes are absent in species without cilia (rice and *Arabidopsis*) and in *C. elegans*, which does not have motile cilia. Future identification of mutations in *Ccdc135* and *FAP50* should shed light on the precise roles of these conserved flagellar proteins. At the present time, we favor a working hypothesis that Pkd2 and CG34110 function in a common signaling pathway: Pkd2 at the level of the flagellar membrane and CG34110 on the axoneme. No calcium- or calmodulin-binding domains are found in CG34110/Ccdc135/FAP50, suggesting that there are intermediary components in the pathway. Identification of the intermediary components will be necessary to fully understand the Pkd2 to CG34110/Ccdc135/FAP50 signaling pathway.

MATERIALS AND METHODS

The sperm storage assay

The sperm storage phenotype can be assayed by direct observation of sperm presence in the female SR. The males to be tested were collected and aged in isolation (1–4 d) before mating with females of the genotype y^1w^1, which has good female fertility. The y^1w^1 females were collected as virgins and aged for at least 2 d before mating with the males. Thirty minutes after mating, the SR tubule along with the uterus was removed by dissection. The SR from a female mated with a wild-type male looks opaque-white due to sperm loading in the DSR. In contrast, the SR from a female mated with a storage-defective mutant male looks transparent due to the lack of sperm in the DSR. The number of sperm in the storage was determined by counting *Protamine-GFP* (Rathke *et al.*, 2007) marked sperm heads in the DSR at 4 and 20 h after mating; similar values

were obtained at both time points for the wild-type sperm (Supplemental Table 1). Thus the mutant sperm in the DSR were counted at 4 h after mating.

The male fertility assay

The sperm storage phenotype can also be assayed by the viable progeny produced per female per mating because the stored sperm is the main source for fertilization, whereas unstored sperm are extruded out of the uterus within 5 h after mating or as soon as the first egg is laid. Collected y^1w^1 female virgins were aged for 3 d in culture vials with added live dry yeast to enhance egg production. The vials holding the female virgins were checked for the presence of larvae before the females were used for the assay. If larvae were found, it meant that some of the females were not virgins and these flies were discarded. The male was separated away from the female immediately after mating, the mated female was allowed to lay eggs, and the viable progeny were counted when they formed pupae on the wall of the culture vial. To examine the temporal pattern of fertility, the mated female was kept in a culture vial for the first 6 or 8 h after mating and then transferred to a new vial for the remaining 10 d. Vials that had no progeny were checked for the presence of eggs. If no eggs were laid, that vial was not included in the tabulation of male fertility because the lack of progeny was the female's fault. Later, the progeny were checked for the expected genotype to make sure that they were fathered by the experimental males.

Genetic identification and mapping of the first *CG34110^{lobo}* allele

Pkd2 mutations result in a severe reduction of sperm accumulation in the female sperm storage organs (Gao *et al.*, 2003). To identify new components of the pathway, we screened Bloomington *Drosophila* stock collections of viable mutations on the third chromosome for reduced sperm storage by the sperm storage assay described above. Information for Bloomington stocks is available from FlyBase (http://flybase.org/). The first *CG34110* allele was identified in Bloomington stock #19168 (w^{1118}; *P(XP)kal-1*^{d01966}). Only the *P(XP)kal-1*^{d01966} homozygous male showed the sperm storage defect, whereas the heterozygote male was wild type in terms of sperm storage. This suggested that the storage defect was caused by a recessive lesion on the *P(XP)kal-1*^{d01966} chromosome. Such a recessive lesion could be caused by the *P(XP)kal-1*^{d01966} insertion or by an unrelated (background) mutation on the same chromosome. To distinguish between these two possibilities, the *P(XP)kal-1*^{d01966} insertion was excised via the P element transposase (*Δ2–3*). The recessive sperm storage defect remained following the precise excision of *P(XP)kal-1*^{d01966}. Thus the sperm storage lesion was due to a separate mutation but located on the *P(XP)kal-1*^{d01966} chromosome.

To map the storage-defective lesion, meiotic recombination was carried out between *P(XP)kal-1*^{d01966} and its proximal marker *P(GT1) CG5346*^{BG02475} (#12694) or its distal markers *P(EP)tankyrase*^{EP3476} (#17132) and *P(SUPor-P)gro*^{KG07117} (#14322). Individual recombinants were tested for the presence of the storage defective lesion in order to calculate its DNA coordinate. The tabulated results showed that the lesion was located ~990 kb distal to *P(XP)kal-1*^{d01966}. The above meiotic recombination analysis also showed that the *P(XP) kal-1*^{d01966} chromosome actually carried two genetic lesions, both independently causing male infertility, but only one located at 3R:20963561..21022720 was causing the sperm storage defect. The other lesion was located at the tip of 3R, which was removed from the *P(XP)kal-1*^{d01966} chromosome by recombination to produce a "clean" sperm storage defective mutation, which we named the lost boys (*lobo*) allele, *CG34110^{lobo}*. *CG34110^{lobo}* fails to complement *CG34110^{MB00722}*, *CG34110^{Q46}* (described later), and *Df(3R)Exel6201*, but complements the adjacent deletion *Df(3R)Exel9056*, for wild-type sperm storage.

Reversion of *CG34110^{MB00722}* by the Minos transposase

CG34110^{MB00722} (#22880) was identified to be allelic to *CG34110^{lobo}* by genetic complementation test, and it contains an engineered transposon *Mi(ET1)* from the Minos transposable element (Metaxakis *et al.*, 2005). To prove that the insertion is causing the sperm storage defect, Minos transposase was introduced into the male germline from *P(hsILMiT)2.4* (#24613). The excision of *Mi(ET1)*, as shown by the loss of the GFP eye marker it carried, reverted the defective sperm storage phenotype back to wild type, indicating that *CG34110^{MB00722}* is a bona fide allele of *CG34110^{lobo}*.

Genetic screen for an additional *CG34110* allele

Because *CG34110* is located at (3R:20963561..21022720), a nearby P element insertion *P(EPgy2)mld*^{EY12290} (3R:20448650; #21378), which had a wild-type sperm storage phenotype and carried a red eye marker, was used to tag the starting chromosome for mutagenesis. Briefly, males carrying the tagged chromosome (w^-; *Tag/TM3*) were treated with 20 mM EMS for 12 h as described (Zhang *et al.*, 1999), and then crossed to female virgins carrying two third chromosome balancers, w^-; *TM2/TM6* (referred to as *T/T*), to ensure the stable transmission of all newly introduced mutations (*) in a balanced genotype of w^-; *Tag*/T*. To identify a new *CG34110* allele, individual (w^-; *Tag*/T*) males were crossed to w^-; *CG34110^{lobo}/T* female virgins, and the male offspring (*Tag*/ CG34110^{lobo}*) were tested in the sperm storage assay described above. One new allele of *CG34110^{Q46}* was identified by screening ~1320 individual mutagenized stocks. The *CG34110^{Q46}* allele produced the storage defect over *CG34110^{lobo}*, *CG34110^{MB00722}*, or *Df(3R)Exel6201*.

DNA sequencing

Genomic DNA samples were isolated from homozygous mutant males (*CG34110^{MB00722}* or *CG34110^{lobo}*), and regions containing exons were amplified by PCR, cloned into pGEM^T, and sequenced. The primers Lobo1F and Lobo2R amplified exons 1–2 (885 bp); Lobo3F and Lobo4R amplified exons 3–4 (922 bp); Lobo5F and Lobo6R amplified exons 5–7 (895 bp); and Lobo7F and Lobo8R amplified exons 8–10 (946 bp). Primer sequences are as follows:

Lobo1F 5′-CTA-ATT-AGA-ATT-ACG-AAA-GTT-TTT-TAA-GC-3′
Lobo2R 5′-GCT-CGG-AAC-ATA-AGA-ATA-ATG-GAT-ATG-TG-3′
Lobo3F 5′-ggt-agt-tga-taa-tcc-agt-ttt-gtc-t-3′
Lobo4R 5′-AGG-AGC-CGA-TGC-AAT-CCA-GGT-GCT-TC-3′
Lobo5F 5′-gaa-gca-cct-gga-ttg-cat-cgg-ctc-ct-3′
Lobo6R 5′-GCC-TGG-AGG-AGA-TTT-AGG-AAT-ACT-TGT-GTG-3′
Lobo7F 5′-cac-aca-agt-att-cct-aaa-tct-cct-cca-ggc-3′
Lobo8R 5′-GGC-AGC-ATA-TCT-TGA-TTA-CCG-AAT-GGA-ATG-G-3′

Antibody production, purification, and uses

Anti-CG34110$^{861–874}$ and anti-CG34110$^{828–842}$ were produced by immunizing rabbits with synthetic peptides derived from the CG34110 sequence, CHEESQKKYEVVKNS-amide (#861–874) and CENQFNNYDYKRLVQQ-amide (#828–842), respectively. Anti-FAP50$^{925–940}$ was produced by immunizing rabbits with the synthetic peptide CRRRDKLRERRVYPQKD-amide (#925–940) of FAP50 from *C. reinhardtii*. Peptide design and immunizing procedures were performed by YenZym Antibodies (San Francisco, CA). The rabbit antisera were purified using affinity resin coupled with the immunizing peptides, by means of a step-wise elution protocol as published (Gao *et al.*,

2003, 2004). The anti-CG34110 antibodies were used at 0.4 µg/ml for Western blotting (Lot 679Af) and 1 µg/ml for sperm staining. The anti-FAP50 antibody was used at a 1:4000 dilution (Lot 681Af-1, salt fraction).

Immunofluorescence microscopy

Mature *Drosophila* sperm from a freshly dissected male SV were spread onto poly-L-lysine–coated glass slides with forceps, covered with a coverslip, and dropped into liquid N_2. After a brief moment in liquid N_2, the coverslip was removed and sperm on the slide were fixed in acetone (−20°C) and methanol (−20°C), successively, for 5 min each, followed by air drying for another 5 min. This fixation protocol (from R. Kamiya) splays the outer doublets of the flagellar axoneme, leading to the exposure of the CG34110 epitope for antibody recognition. Fixation of sperm with 4% formaldehyde did not work for this antigen. Following air drying, the slide was rehydrated in PBT and treated with Image-iT FX Signal Enhancer (Molecular Probes, Eugene, OR) for 30 min, then processed for immunostaining as published (Gao *et al.*, 2003). The anti-CG34110 antibody was either anti-CG34110$^{861–874}$ or anti-CG34110$^{828–842}$ (1 µg/ml), and the secondary antibody was Alexa Fluor 594 goat anti–rabbit immunoglobulin (Ig) (H+L) conjugate (A-11037; Molecular Probes). The blocking solution was StartingBlock blocking buffer from Pierce (Rockford, IL).

Characterization of sperm orientation in the reproductive tract

Sperm orientation in the reproductive tract was imaged by using the GFP markers *Protamine-GFP* (Rathke *et al.*, 2007) and *Dj-GFP* (Gao *et al.*, 2003; Santel *et al.*, 1997) (obtained from B.T. Wakimoto and R. Renkawitz-Pohl) that label the sperm head and tail, respectively. Images were captured on a Nikon multizoom AZ100 microscope with a magnification range of 10×–320× using the Nikon NIS-Elements imaging software. The microscope was fitted with a Nikon Intensilight 130W High-Pressure Mercury Lamp, a GFP HC HiSN Zero Shift Filter set with excitation wavelength (450–490 nm), dichroic mirror (495 nm), and emission filter (500–550 nm), and a Photometrics Coolsnap EZ 12-Bit Cooled CCD monochrome camera.

To visualize sperm in the male or female reproductive tract, sperm movement was induced by male–female conjugation, which results in the movement of sperm from the male SV, where mature sperm are stored, to the male ED and then to the uterus of the conjugating female. The sperm in the uterus then move into the 2-mm-long female SR tubule and eventually return back out of the SR for fertilization. To observe specific stages in this sequence of events, liquid N_2 or dry ice was used to freeze the conjugating pair of flies at various times following copulation. To set up mating, one y^1w^1 female virgin was added to a vial that already contained one male to be analyzed. Mating usually initiated within minutes to 1 h after adding the female. The starting time of copulation was noted, and the copulating pair of flies was fast-frozen at various time points depending on the type of sperm movement to be observed. Then, the relevant tissues were dissected out of the frozen flies and imaged. All tissue dissections were carried out in 50% *Drosophila* Ringer's solution at final concentrations of 91 mM KCl, 23 mM NaCl, 1.5 mM $CaCl_2$, and 5 mM Tris-Cl, pH 7.2. Tissues were not fixed, and imaging was done immediately after tissue dissection.

To observe sperm movement from the SV into the ED, copulating flies were fast-frozen at 2–6 min after the onset of copulation and the male reproductive tract was dissected either immediately or 1–2 d later. To ensure that sperm were not artificially dislodged, spacers were placed between the slide and coverslip. The use of young virgin males (1–2 d old) has been effective for avoiding the complication of residual sperm tails in the ED, which could come from a previous mating or sperm leakage that is known to occur as crystal condensate at the male external genitalia. For live imaging, the male reproductive tract was dissected as fast as possible and mounted on the slide for video recording using the Nikon NIS-Elements imaging software.

To quantify sperm orientation at the PSR entry, mating was terminated by freezing the flies at 15 min after the onset of copulation. This time is near the beginning of sperm entry into the SR, and it is too short of a time for any sperm to fully enter the SR and then come back out. The female reproductive tract was dissected but not fixed to aid in the uncoiling of the naturally coiled SR tubule by forceps. To be counted as a leading structure, the head or tail had to move ≥0.1 mm into the SR tubule. To be counted as "tangled" sperm, the sperm had to be folded at least once. To observe sperm exit out of the SR, the mated females were allowed to lay eggs for 24 h following mating before the females were fast-frozen for imaging. In our experiments, the females generally start to lay fertilized eggs between 5 and 6 h after mating. Many eggs produced in the first 24 h hatched, indicating that the 24-h time point was appropriate for observing the SR exit movement of sperm.

To observe sperm movement inside the uterus, the inseminated uterus was dissected out of the female between 10 and 30 min following mating completion. Sperm are extremely sensitive to mechanical stimulation. We avoided poking the uterine wall as this was found to stop all sperm movement inside the uterus. Video was captured by the Nikon NIS-Elements software using the "continuous" mode (see Supplemental Movie legend for video speed).

To observe sperm movement inside the DSR, the uterus from a mated female was mounted on a slide. Without further manipulation, the DSR is already exposed and ready for imaging. For wild-type sperm, the large number of sperm stored prohibits a clear observation of sperm movement in the DSR. To overcome this, successive mating of one male with multiple females was used to reduce the sperm number in the receptacle.

Isolation, fractionation, and Western blotting of *C. reinhardtii* flagella

C. reinhardtii strains *137c* (wild type), *pf14*, *pf18*, *mbo1* (CC2679), *mbo2* (CC3664), and *mbo3* (CC2378) were grown as described (Witman, 1986). For comparison of these strains, flagella and axonemes were isolated as described (Witman, 1986) with the following modifications. For comparison of wild type and the *mbo* mutants, EGTA instead of Na_2EDTA was used in the HMDEK solution and a 1:100 dilution of Plant Protease Inhibitor Cocktail (Sigma P9599, St. Louis, MO) was added to the solution. The same method was used for the comparison of wild type, *pf14*, and *pf18*, except that dithiothreitol (DTT) was excluded from the HMDS solution and the protease inhibitor was omitted from the HMDEK solution.

For the analysis of wild-type flagellar fractions, cells from a 4-l culture (midlog phase) were resuspended in ~100 ml of 10 mM HEPES, pH 7.0. The cells were deflagellated by adding 0.5 M acetic acid to pH 4.5; 30 s later, 0.5 M KOH was added to bring the pH back to 7.0. The cells were placed on ice immediately after deflagellation, and then 1 M $MgSO_4$, 1 M DTT, 50% sucrose, 0.5 M EDTA, 100 mM phenylmethylsulfonyl fluoride (PMSF), and 1 M HEPES at pH 7.0 were added in that order to yield final concentrations of 5 mM $MgSO_4$, 1 mM DTT, 5% sucrose, 0.25 mM EDTA, 1 mM PMSF, and 10 mM HEPES. A 150-ml cell suspension in 250-ml tubes was underlain with 50 ml of 25% sucrose in HMDE (10 mM HEPES, 5 mM

$MgSO_4$, 1 mM DTT, 0.25 mM EDTA) and centrifuged at 853 × *g* for 5 min at 4°C. The supernatant was collected and the flagella harvested by centrifugation at 11,950 × *g* for 10 min at 4°C. Flagellar fractionation was as previously described (Pazour *et al.*, 1999), except that Plant Protease Inhibitor Cocktail (Sigma P9599, used 1:100) was added to the flagella and all extraction solutions immediately prior to demembranation.

SDS–PAGE and Western blotting were as previously described (Pazour *et al.*, 1999). In addition to anti-FAP50 (see above), antibodies used to probe Western blots were rabbit polyclonal anti-IFT46 (Hou *et al.*, 2007) and mouse monoclonal anti-IC2 (King *et al.*, 1985).

ACKNOWLEDGMENTS

This research is funded by NIH DK071073 and PKD Research Foundation to X.L., and by NIH GM030626 and funds from the Robert W. Booth Endowment to G.B.W.; G.B.W. is a member of the UMass DERC (DK32520). W.F.M. acknowledges support from the W.M. Keck Foundation. We thank R. Kamiya for sharing flagellar staining protocol, E. Spana at Duke Model System Genomics for microarray experiments, T. McClintock for information on GM770, B.T. Wakimoto and R. Renkawitz-Pohl for sperm GFP reporters, the Bloomington *Drosophila* Stock Center for fly stocks, R. Patten and R. Lillich for Nikon microscopic imaging, and D. Neumann for video processing. The Microscopy and Imaging Resources Laboratory is supported, in part, by NIH Center Grants P30ES06639 to the Institute of Environmental Health Sciences, P30CA22453 to the Karmanos Cancer Institute, and U54RR020843 to the Center for Proteolytic Pathways, the Burnham Institute and the Perinatology Research Branch of the NICHD, Wayne State University.

REFERENCES

Baccetti B, Gibbons BH, Gibbons IR (1989). Bidirectional swimming in spermatozoa of Tephritid flies. J Submicrosc Cytol Pathol 21, 619–625.

Baker K, Beales PL (2009). Making sense of cilia in disease: the human ciliopathies. Am J Med Genet C Semin Med Genet 151C, 281–295.

Barr MM, Sternberg PW (1999). A polycystic kidney-disease gene homologue required for male mating behaviour in C. elegans. Nature 401, 386–389.

Bessen M, Fay RB, Witman GB (1980). Calcium control of waveform in isolated flagellar axonemes of Chlamydomonas. J Cell Biol 86, 446–455.

Bloch Qazi MC, Wolfner MF (2006). Emergence of sperm from female storage sites has egg-influenced and egg-independent phases in Drosophila melanogaster. Biol Lett 2, 128–130.

Braiman A, Priel Z (2008). Efficient mucociliary transport relies on efficient regulation of ciliary beating. Respir Physiol Neurobiol 163, 202–207.

Brokaw CJ (2006). Flagellar propulsion. 1955. J Exp Biol 209, 985–986.

Chintapalli VR, Wang J, Dow JA (2007). Using FlyAtlas to identify better Drosophila melanogaster models of human disease. Nat Genet 39, 715–720.

Dymek EE, Smith EF (2007). A conserved CaM- and radial spoke associated complex mediates regulation of flagellar dynein activity. J Cell Biol 179, 515–526.

Eisenbach M, Giojalas LC (2006). Sperm guidance in mammals—an unpaved road to the egg. Nat Rev Mol Cell Biol 7, 276–285.

Gao Z, Joseph E, Ruden DM, Lu X (2004). Drosophila Pkd2 is haploid-insufficient for mediating optimal smooth muscle contractility. J Biol Chem 279, 14225–14231.

Gao Z, Ruden DM, Lu X (2003). PKD2 cation channel is required for directional sperm movement and male fertility. Curr Biol 13, 2175–2178.

Gibbons IR (1981). Cilia and flagella of eukaryotes. J Cell Biol 91, 107s–124s.

Goodenough UW, Heuser JE (1989). Structure of the soluble and in situ ciliary dyneins visualized by quick-freeze deep-etch microscopy. In: In Movement, eds. FD Warner, P Satir, IR Gibbons, New York: Alan R. Liss, 121–140.

Guo R, Ma PP, Ma J, Ge YH, Xue SP, Han DS (2004). Cloning and characterization of a novel gene SRG-L expressed in late stages of mouse spermatogenic cells. Acta Biochim Biophys Sin (Shanghai) 36, 315–322.

Heuser T, Raytchev M, Krell J, Porter ME, Nicastro D (2009). The dynein regulatory complex is the nexin link and a major regulatory node in cilia and flagella. J Cell Biol 187, 921–933.

Hill KL (2003). Biology and mechanism of trypanosome cell motility. Eukaryot Cell 2, 200–208.

Hou Y, Qin H, Follit JA, Pazour GJ, Rosenbaum JL, Witman GB (2007). Functional analysis of an individual IFT protein: IFT46 is required for transport of outer dynein arms into flagella. J Cell Biol 176, 653–665.

Huang K, Diener DR, Mitchell A, Pazour GJ, Witman GB, Rosenbaum JL (2007). Function and dynamics of PKD2 in Chlamydomonas reinhardtii flagella. J Cell Biol 179, 501–514.

Immler S (2008). Sperm competition and sperm cooperation: the potential role of diploid and haploid expression. Reproduction 135, 275–283.

Ishijima S, Hamaguchi Y (1993). Calcium ion regulation of chirality of beating flagellum of reactivated sea urchin spermatozoa. Biophys J 65, 1445–1448.

Ishijima S, Ishijima SA, Afzelius BA (1994). Movement of Myzostomum spermatozoa: calcium ion regulation of swimming direction. Cell Motil Cytoskeleton 28, 135–142.

Ishijima S, Ishijima SA, Afzelius BA (1999). Movement of turritella spermatozoa: direction of propagation and chirality of flagellar bends. Cell Motil Cytoskeleton 44, 85–95.

Kagami O, Kamiya R (1990). Strikingly low ATPase activities in flagellar axonemes of a Chlamydomonas mutant missing outer dynein arms. Eur J Biochem 189, 441–446.

Kagami O, Kamiya R (1992). Translocation and rotation of microtubules caused by multiple species of Chlamydomonas inner-arm dynein. J Cell Sci 103, 653–664.

Karr TL, Pitnick S (1996). The ins and outs of fertilization. Nature 379, 405–406.

Kaupp UB, Kashikar ND, Weyand I (2008). Mechanisms of sperm chemotaxis. Annu Rev Physiol 70, 93–117.

King SM, Otter T, Witman GB (1985). Characterization of monoclonal antibodies against Chlamydomonas flagellar dyneins by high-resolution protein blotting. Proc Natl Acad Sci USA 82, 4717–4721.

King SM (2010). Sensing the mechanical state of the axoneme and integration of Ca2 +signaling by outer arm dynein. Cytoskeleton (Hoboken) 67, 207–213.

King SM, Otter T, Witman GB (1986). Purification and characterization of Chlamydomonas flagellar dyneins. Methods Enzymol 134, 291–306.

Lechtreck K-F, Delmotte, P, Robinson ML, Sanderson MJ, Witman GB (2008). Mutations in *Hydin* impair ciliary motility in mice. J Cell Biol 180, 633–643.

Lyons RA, Saridogan E, Djahanbakhch O (2006). The reproductive significance of human Fallopian tube cilia. Hum Reprod Update 12, 363–372.

Ma Q, Wang H, Guo R, Wang H, Ge Y, Ma J, Xue S, Han D (2006). Molecular cloning and characterization of SRG-L, a novel mouse gene developmentally expressed in spermatogenic cells. Mol Reprod Dev 73, 1075–1083.

Manier MK, Belote JM, Berben KS, Novikov D, Stuart WT, Pitnick S (2010). Resolving mechanisms of competitive fertilization success in Drosophila melanogaster. Science 328, 354–357.

McClintock TS, Glasser CE, Bose SC, Bergman DA (2008). Tissue expression patterns identify mouse cilia genes. Physiol Genomics 32, 198–206.

Metaxakis A, Oehler S, Klinakis A, Savakis C (2005). Minos as a genetic and genomic tool in Drosophila melanogaster. Genetics 171, 571–581.

Miller GT, Pitnick S (2002). Sperm-female coevolution in Drosophila. Science 298, 1230–1233.

Mirzadeh Z, Han YG, Soriano-Navarro M, García-Verdugo JM, Alvarez-Buylla A (2010). Cilia organize ependymal planar polarity. J Neurosci 30, 2600–2610.

Mitchell D (2007). The evolution of eukaryotic cilia and flagella as motile and sensory organelles. Adv Exp Med Biol 607,130–140.

Mitchell DR (2004). Speculations on the evolution of 9+2 organelles and the role of central pair microtubules. Biol Cell 96, 691–696.

Naito Y, Kaneko H (1972). Reactivated triton-extracted models o paramecium: modification of ciliary movement by calcium ions. Science 176, 523–524.

Neubaum DM, Wolfner MF (1999). Mated Drosophila melanogaster females require a seminal fluid protein, Acp36DE, to store sperm efficiently. Genetics 153, 845–857.

Norrander JM, deCathelineau AM, Brown JA, Porter ME, Linck RW (2000). The Rib43a protein is associated with forming the specialized protofilament ribbons of flagellar microtubules in Chlamydomonas. Mol Biol Cell 11, 201–215.

Okada Y, Nonaka S, Tanaka Y, Saijoh Y, Hamada H, Hirokawa N (1999). Abnormal nodal flow precedes situs inversus in iv and inv mice. Mol Cell 4, 459–468.
Parry DA, Fraser RD, Squire JM (2008). Fifty years of coiled-coils and alpha-helical bundles: a close relationship between sequence and structure. J Struct Biol 163, 258–269.
Pazour GJ, Agrin N, Leszyk J, Witman GB (2005). Proteomic analysis of a eukaryotic cilium. J Cell Biol 170, 103–113.
Pazour GJ, Dickert BL, Witman GB (1999). The DHC1b (DHC2) isoform of cytoplasmic dynein is required for flagellar assembly. J Cell Biol 144, 473–481.
Pennekamp P, Karcher C, Fischer A, Schweickert A, Skryabin B, Horst J, Blum M, Dworniczak B (2002). The ion channel polycystin-2 is required for left-right axis determination in mice. Curr Biol 12, 938–943.
Pfister KK, Fay RB, Witman GB (1982). Purification and polypeptide composition of dynein ATPases from Chlamydomonas flagella. Cell Motil 2, 525–547.
Piperno G, Ramanis Z, Smith EF, Sale WS (1990). Three distinct inner dynein arms in Chlamydomonas flagella: molecular composition and location in the axoneme. J Cell Biol 110, 379–389.
Porter ME, Sale WS (2000). The 9 + 2 axoneme anchors multiple inner arm dyneins and a network of kinases and phosphatases that control motility. J Cell Biol 151, F37–F42.
Publicover SJ, Giojalas LC, Teves ME, de Oliveira GS, Garcia AA, Barratt CL, Harper CV (2008). Ca2+ signalling in the control of motility and guidance in mammalian sperm. Front Biosci 13, 5623–5637.
Rathke C, Baarends WM, Jayaramaiah-Raja S, Bartkuhn M, Renkawitz R, Renkawitz-Pohl R (2007). Transition from a nucleosome-based to a protamine-based chromatin configuration during spermiogenesis in Drosophila. J Cell Sci 120, 1689–1700.
Santel A, Winhauer T, Blumer N, Renkawitz-Pohl R (1997). The Drosophila don juan (dj) gene encodes a novel sperm specific protein component characterized by an unusual domain of a repetitive amino acid motif. Mech Dev 64, 19–30.
Satir P, Mitchell DR, Jekely G (2008). How did the cilium evolve? Curr Top Dev Biol 85, 63–82.
Sawamoto K *et al.* (2006). New neurons follow the flow of cerebrospinal fluid in the adult brain. Science 311, 629–632.
Schmidt JA, Eckert R (1976). Calcium couples flagellar reversal to photostimulation in Chlamydomonas reinhardtii. Nature 262, 713–715.
Segal RA, Huang B, Ramanis Z, Luck DJ (1984). Mutant strains of Chlamydomonas reinhardtii that move backward only. J Cell Biol 98, 2026–2034.
Smith EF (2002a). Regulation of flagellar dynein by calcium and a role for an axonemal calmodulin and calmodulin-dependent kinase. Mol Biol Cell 13, 3303–3313.
Smith EF (2002b). Regulation of flagellar dynein by the axonemal central apparatus. Cell Motil Cytoskeleton 52, 33–42.
Smith EF, Yang P (2004). The radial spokes and central apparatus: mechano-chemical transducers that regulate flagellar motility. Cell Motil Cytoskeleton 57, 8–17.
Snook RR, Karr TL (1998). Only long sperm are fertilization-competent in six sperm-heteromorphic Drosophila species. Curr Biol 8, 291–294.
Sugrue P, Hirons MR, Adam JU, Holwill ME (1988). Flagellar wave reversal in the kinetoplastid flagellate Crithidia oncopelti. Biol Cell 63, 127–131.
Tam LW, Lefebvre PA (2002). The Chlamydomonas MBO2 locus encodes a conserved coiled-coil protein important for flagellar waveform conversion. Cell Motil Cytoskeleton 51, 197–212.
Venglarik CJ, Gao Z, Lu X (2004). Evolutionary conservation of Drosophila polycystin-2 as a calcium-activated cation channel. J Am Soc Nephrol 15, 1168–77.
Vogel P, Read R, Hansen GM, Freay LC, Zambrowicz BP, Sands AT (2010). Situs inversus in Dpcd/Poll-/-, Nme7-/- , and Pkd1l1-/- mice. Vet Pathol 47, 120–131.
Walker PJ (1961). Organization of function in trypanosome flagella. Nature 189, 1017–1018.
Wang Q, Pan J, Snell WJ (2006). Intraflagellar transport particles participate directly in cilium-generated signaling in Chlamydomonas. Cell 125, 549–562.
Wang Q, Snell WJ (2003). Flagellar adhesion between mating type plus and mating type minus gametes activates a flagellar protein-tyrosine kinase during fertilization in Chlamydomonas. J Biol Chem 278, 32936–32942.
Watnick TJ, Jin Y, Matunis E, Kernan MJ, Montell C (2003). A flagellar polycystin-2 homolog required for male fertility in Drosophila. Curr Biol 13, 2179–2184.
Werner M, Simmons LW (2008). Insect sperm motility. Biol Rev Camb Philos Soc 83, 191–208.
Wilson GR, Wang HX, Egan GF, Robinson PJ, Delatycki MB, O'Bryan MK, Lockhart PJ (2010). Deletion of the Parkin co-regulated gene causes defects in ependymal ciliary motility and hydrocephalus in the quakingviable mutant mouse. Hum Mol Genet 19, 1593–1602.
Witman GB (1986). Isolation of Chlamydomonas flagella and flagellar axonemes. Methods Enzymol 134, 280–290.
Wu G *et al.* (1998). Somatic inactivation of Pkd2 results in polycystic kidney disease. Cell 93, 177–188.
Yagi T, Uematsu K, Liu Z, Kamiya R (2009). Identification of dyneins that localize exclusively to the proximal portion of Chlamydomonas flagella. J Cell Sci 122, 1306–1314.
Yang Y, Lu X (2011). Drosophila sperm motility in the reproductive tract. Biol Reprod (*in press*). Published online Feb 3, 2011.
Zhang Q, Zheng Q, Lu X (1999). A genetic screen for modifiers of drosophila Src42A identifies mutations in Egfr, rolled and a novel signaling gene. Genetics 151, 697–711.